Effects of ultrasound on colloidal organization at nanometer length scale during cross-flow ultrafiltration probed by in-situ SAXS

Yao Jin, Nicolas Hengl, Stéphane Baup, Frédéric Pignon, Nicolas Gondrexon, Albert Magnin, Michael Sztucki, Theyencheri Narayanan, Laurent Michot, Bernard Cabane

Effects of ultrasound on colloidal organization at nanometer length scale during cross-flow ultrafiltration probed by *in-situ* SAXS

JIN Yao[a], HENGL Nicolas [a], BAUP Stéphane[a], PIGNON Frédéric[a*], GONDREXON Nicolas[a], MAGNIN Albert[a], SZTUCKI Michael[b], NARAYANAN Theyencheri[b], MICHOT Laurent[c], CABANE Bernard[d]

[a] Laboratoire Rhéologie et Procédés, U.J.F. Grenoble I, Grenoble - INP, CNRS, UMR 5520, BP 53, Domaine universitaire, 38041 Grenoble Cedex 9, France
[b] European Synchrotron Radiation Facility, BP220 38043 Grenoble Cedex 9, France

[c] Laboratoire Interdisciplinaire des Environnements Continentaux. PECSA UMR 7195 - CNRS - UPMC – ESPCI, 4 place Jussieu, case courrier 51 75005 Paris Cedex 5, France

[d]Laboratoire PMMH, ESPCI, 10 Rue Vauquelin, 75231 Paris Cedex 5, France

Abstract

Effects of ultrasound (US) on the structural organization within concentrated particles layer during cross-flow utrafiltration of Laponite dispersions have been characterized for the first time by *in-situ* time-resolved small-angle X-ray scattering (SAXS). A novel ‘‘SAXS Cross-Flow US-coupled Filtration Cell’’ has been developed to, on one hand, apply ultrasonic waves close to the flat membrane by embedding in the feed compartment a thin titanium vibrating blade connected to a 20 kHz ultrasonic generator and on the other hand, to monitor *in-situ* the colloidal organization of the concentrated layer by SAXS. Thanks to this cell, concentration profiles have been measured as a function of the distance z from the membrane surface with a 20 µm accuracy and simultaneously linked to the permeate flux, cross-flux and transmembrane pressure. *In-situ* ultrasonication leads to a significant increase of permeate flux arising from the break-up of the concentrated layer. Results also suggest that ultrasonication could be considered as an additional force of an effective range on the order of micrometers or smaller. It is capable to completely remove the particles from the membrane surface when the feed dispersions are dense and aggregated, and is more efficient than classical procedures based on an increase of the cross-flow flux.

Keywords: ultrafiltration, ultrasound, fouling layer, SAXS, Laponite

*Corresponding authors: frederic.pignon@ujf-grenoble.fr, nicolas.hengl@ujf-grenoble.fr

1. INTRODUCTION

Membrane separation processes are used to concentrate, purify or remove solute from solution. It is currently a proven technology within many important areas, such as food and dairy industries, water purification and treatment of liquid fluent streams. Cross-flow ultrafiltration is one of the most popular developments in membrane technology. Although it presents numerous advantages (large active area per unit volume, easy to operate, multiple configurations and modularity), this technology is mainly limited by the accumulation of matter on the membrane surface which leads to two phenomena: concentration polarization [1] and membrane fouling [2]. Several techniques have been developed trying to overcome these limitations but all of them present drawbacks [3–5].

Ultrasound (US) is an efficient tool in several areas of industrial process engineering. It is based on ultrasonic waves propagation within the liquid, leading to the combined effect of cavitation, acoustic streaming, etc. [6]. The application of ultrasound in conventional membrane filtration has been investigated and various studies report process enhancement. Research has often been carried out during membrane cleaning process [7–11] but online ultrasonication has also been applied in both cross-flow [8,10,12–15] and dead-end filtration [16]. In most of these studies, the ultrasound devices are ultrasonic water baths, in which the loss of acoustic power is reported to be very high, about 90% [17]. In order to have a better control of US, Simon *et al.* (2000) [16] , Juang *et al.* (2004) [18] and Mirzaie and Mohammadi (2012) [19] used an ultrasonic probe system to transmit ultrasonic waves directly to the feed medium in a dead-end filtration operation. Kyllönen et *al*. (2006) [13] also developed a membrane module integrated with several sandwich type ultrasonic transducers to apply ultrasound in cross-flow filtration with little loss of ultrasonic efficiency. Using a different approach than that developed by Kyllönen et *al*. (2006), the present study proposes a new ultrasonic-assisted cross-flow membrane filtration module that can apply ultrasonication directly on the feed side of the membrane at a very close distance (8 mm).

To understand the mechanism of ultrasonic enhancement of membrane filtration, different approaches have been used. Due to its ease of measurement, the evolution of permeate flux is the most obvious measurement to carry out and is directly linked to filtration performance. However it does not provide any information on mechanisms occurring within the concentrated particles layer (including reversible concentration polarization layer and irreversible fouling layer) in the feed. Filtrate concentrations close to the membrane surface as well as mass transfer coefficients within the concentrated layer under ultrasonication have been estimated using theoretical and modeling approaches [14,20] whereas Scanning Electron Microscopy (SEM) has been used to characterize ‘‘offline’’ the fouling cake formed during filtration with and without ultrasound [6,19]. Still, to our knowledge, no real time observation of the concentrated layers during cross-flow filtration under ultrasonication has ever been reported.

To reach such a goal, small-angle X-ray scattering (SAXS) measurements were carried out at the European Synchrotron Radiation Facility (ESRF, ID02 High Brilliance SAXS/WAXS/USAXS Beamline). A novel ‘‘SAXS Cross-Flow US-coupled Filtration Cell’’ has been especially developed at the “Laboratoire Rhéologie et Procédés”, which allows characterizing, *in-situ*, the induced structures and concentration profiles in the vicinity of the ultrafiltration membranes at nanometer length scales over time, when feed dispersions are simultaneously subjected to a transmembrane pressure, cross-flow over the membrane and ultrasonication. The colloidal dispersions filtered are synthetic aqueous clay Laponite, already used in our previous work [21]. In these previous experiments, the dispersions were studied by *in-situ* SAXS during ultrafiltration, but without the ability to apply ultrasound. The Laponite dispersions used here, consisting of nanometric platelets, with shear-thinning rheological behavior for the volume fractions and physico-chemical conditions studied in the present paper.

This work combines macroscopic results with simultaneous observations at nanometer length scale during ultrafiltration. To the best of our knowledge, it is the first time that the effect of ultrasound on cross-flow filtration is determined by *in-situ* characterization of the concentration profiles and structural organization within concentrated particles layer over time.

2. MATERIALS AND METHODS

2.1 Sample preparation

Laponite XLG, manufactured by Laponite Industries, was employed in this paper. Laponite XLG dispersions were prepared under high shear in demineralized water at 20 °C at a fixed ionic strength of 10^{-3} M NaCl. Suspended Laponite particles are in the form of roughly circular discs with a diameter of 25-30 nm and thickness of 1-2 nm [22]. Dispersions to be filtered were prepared at initial volume fractions of ϕ_v=0.48% and 1%, corresponding to mass fraction of 0.0121 g.cm^3 and 0.0253 g.cm^3, respectively. The dispersions were then aged in closed vessels for 12-26 days before the filtration experiments. The pH value of the dispersions remained stable during this aging time and equal to 10 during the measurement, which indicates that there is no further dissolution of material since the pH was always above 9 [23]. The structure and rheological properties of these dispersions evolve with time [23,24]. Consequently, the time tp that elapsed between the end of preparation and the investigations will always be indicated in this paper. A peptizer, tetrasodium diphosphate $Na_4P_2O_7$ (tspp) was added to the dispersions with a concentration of 6 % (percentage with regard to dry clay mass), the peptizer concentration is denoted as Cp. The effect of this peptizer on the structure, rheological behavior, osmotic pressure and frontal filtration performance of the Laponite dispersions has been studied in previous works [24–26]. A reduction in attractive force between the particles takes

place while adding this peptizer, which leads to a transformation of the flow properties from yield stress gels to shear-thinning fluids, as those investigated dispersions in this study.

2.2 Rheometric measurements

The rheological behavior of the dispersions was studied with a shear rate controlled rheometer (ARG2, TA Instrument) with a stainless steel cone and plate geometry (diameter 49 mm, angle 4°21'). In order to avoid interfacial effects, the surfaces of the apparatus were covered with sand-paper with a roughnes of 200 µm. Measurements were carried out at a temperature of 25±1°C. The atmosphere around the sample was saturated with water to prevent evaporation during the measurement [27].

2.3 'SAXS Cross-Flow US-coupled Filtration' cell and filtration procedure

2.3.1 Filtration setup and procedure

Previously, a 'SAXS Cross-Flow Filtration Cell' was developed to measure *in-situ* the concentration and structural organization of colloids as a function of time at different distances z from the membrane surface [21]. This cell is made of transparent polycarbonate and contains a flat polyethersulfone ultrafiltration membrane (100 kD, PleyadeRayflow x100, Rhodia Orelis). The design of this filtration cell was modified in order to combine an ultrasound system: a thin titanium vibrating blade was embedded in the feed compartment and placed above the flat membrane at a distance of 8 mm. This blade is connected to a sonotrode consisting of a piezoelectric transducer attached to a metal rod, which generates ultrasonic waves at a 20 kHz frequency and at an applied amplitude of 1.6 µm (SODEVA TDS, France). The input electric power stretches from 2 W to 10 W, corresponding to power intensity from 0.57 $W.cm^{-2}$ to 2.86 $W.cm^{-2}$ (the input power per unit area of the blade surface). What will be indicated in the following sections refers to the input electric power; about 70% of it is transmitted to effective ultrasonic power. The feed channel is 100 mm long in tangential flow direction and 4 mm × 8 mm (width ×height) in the flow section. Three windows of 3 mm × 5.5 mm × 0.3 mm (width × height × thickness) are opened into the wall located upstream, in the middle and downstream in the feed compartment with a distance of 43 mm from each other (Fig. 1a). The filtration cell was mounted in a motorized stage, which allows monitoring by SAXS the concentration and structural organization of suspensions at different distances from the membrane as well as at different positions along the membrane.

As shown in Fig. 1b, during filtration, the feed suspensions, denoted as retentate, are pumped (Mono pump LF series) from a high pressure resistant vessel (Millipore) to the filtration cell and the cross-flow flux is quantified constantly by a magnetic flow meter (Optiflux 6300C, Krohne). The pressure is applied via purified compressed air, and is monitored by two pressure gauges (FP 110 FGP Sensors & Instrument) at both the inlet and outlet of the filtration cell. The filtration temperature is maintained at 25°C by a thermostatic bath (Thermo &Scientific SC 150 A25, HAAKE) and it is verified constantly

by two sensors (YC-747D with K thermocouples) at both inlet and outlet of the filtration cell. The permeate flux J_v is monitored by measuring the mass variation in the reservoir vessel every 5 s with an accuracy of 0.001 g (Balance Precisa 400M).

2.3.2 SAXS measurement conditions and analysis

SAXS measurements were carried out at the ID02 High Brilliance SAXS/WAXS/USAXS Beamline [28], at the European Synchrotron Radiation Facility (ESRF, Grenoble, France). The incident X-ray beam of wavelength (λ) 0.1 nm, was collimated to 20 µm vertically and 200 µm horizontally using slits. Two sample-to-detector distances were used which provided a scattering vector **q** range from 0.01 nm^{-1} to 6 nm^{-1}, where $q = (4\pi/\lambda) \sin(\theta/2)$ with θ the scattering angle, which corresponds to a length scale range ($l = 2\pi/q$) from 1 nm to 600 nm. The incident beam passed through the sample and the two-dimensional scattered intensity patterns were recorded on a high-resolution CCD detector. Measured scattering patterns were normalized to an absolute intensity scale after applying standard detector corrections and then azimuthally averaged to obtain the one-dimensional intensity profiles denoted by I(q). The normalized background scattering of the different cells filled with distilled water was systematically subtracted [21,29] from the corresponding sample scattered intensities. While some qualitative information could be directly obtained from the two-dimensional patterns such as the anisotropy and orientation of particles, quantitative modeling of I(q) provides the mean particle size, shape and their structural arrangement [29].

To characterize the initial suspensions, SAXS measurements on 5 dispersions of known volume fractions were performed in a temperature controlled (25±1 °C) flow-through capillary cell (diameter ~ 2 mm). This allowed establishing a relationship between the scattering intensities and the volume fractions, leading to a calibration curve. *In-situ* measurements were performed using the cross-flow filtration cell depicted in Fig. 1. The distance z from the membrane [29] was accurately mapped by transmitted intensity measurements. The minimum distance above the membrane for obtaining exploitable SAXS data was about 20 µm.

3. RESULTS AND DISCUSSIONS

In this section, the effect of ultrasonication on cross-flow ultrafiltration of Laponite dispersions is determined. First of all, the ultrasonic effect on Laponite dispersions properties will be presented. Secondly, the effect of ultrasound on filtration performance at macro-scale has been determined. The third part presents the colloidal organization of Laponite at nanometer length scale during this ultrasonic-assisted filtration probed by SAXS.

3.1 Effect of ultrasonication on Laponite dispersions properties

Two approaches were adopted to detect the effect of ultrasound on Laponite dispersions properties during filtration: rheometric and SAXS measurements. In Fig. 2a the steady state flow curves of Laponite dispersions (ϕ_v = 1%) are plotted. For each suspension, four samples were analyzed: one at rest and three others were taken from bulk dispersions during cross-flow filtration with/without ultrasound, the rheological behaviors being determined 5 minutes after sampling. For the dispersions at rest, which are not subjected to the shear stress of pump in the filtration setup, a shear thinning fluid behavior can be observed and the stress levels at all shear rates are relatively high. When submitted to a strong shear stress resulting from the pump, the dispersion flows more easily, especially at lower shear rates where the stress levels are reduced by two orders of magnitude, as demonstrated by the curve of filled circles in Fig. 2a. These results indicate that the network of mechanical links of Laponite dispersions has been weakened or dissociated by the additional shear stress (the pump). In fact, this kind of dispersions flows over time when shaken, agitated, otherwise stressed, due to their thixotropic behavior [24]. It has been reported that Laponite dispersions often take several hours to return to their initial higher viscosity, which leaves us enough time to carry out the rheological measurements [30]. After 40 min of conventional filtration, ultrasonic waves were applied simultaneously for another 40 min. We noticed that a 40 min ultrasonication did not have a marked influence on the dispersions already sheared by the pump, but additional break-up could still be observed. Indeed, without any change in the shear-thinning behavior, the shear stresses decrease at given shear rates; when ultrasound was switched off, the shear stresses then increased slightly as shown by the curve with triangles.

Figure 2b presents the SAXS intensities of Laponite dispersions as a function of scattering vector q. In order to reveal the ultrasonic effect on the structure of Laponite dispersions during filtration, the scattering intensities of two dispersions at 2 vol% with and without ultrasonication during filtration and one at rest, were compared. The sample at rest was analyzed in the capillary flow-through cell. It is obvious that the structure has been modified by shear stress at the length scales of interparticles ($0.01\ nm^{-1} \leq q \leq 0.2\ nm^{-1}$, corresponding to length scales between 600 nm and 30 nm). Such shape change of scattering intensities curve (between the circles and the others) at short range of q vectors (below $0.2\ nm^{-1}$) could be explained by the fact that the mutual interaction between the particles has decreased, noting that the mechanical properties of Laponite dispersions are controlled by a network of aggregates [23]. However, no effective influence of ultrasonication on Laponite structure was observed on the scattering intensity in this q range (Fig. 2b). This is probably due to the fact that both samples were already subjected to ultrasound before (the samples were picked up at step 7 and 8, as described in section 3.3.2) and the dispersions were then already disaggregated. Otherwise, no modification of the size and shape of the particles caused by ultrasonication can observed since the scattering intensities of all three samples are exactly the same at the length scales of particles (above $0.2\ nm^{-1}$, corresponding to a length of 30 nm, the average diameter of Laponite discs).

3.2 Effect of ultrasonication on cross-flow ultrafiltration performance at macro-scale

An alternating increase-decrease transmembrane pressure filtration procedure, proposed by Espinasse et *al.*[31], was used to identify concentration polarization phenomena and membrane fouling during filtration. Using such a procedure, reversible fouling can be distinguished from deposit at the range of applied pressure. It also illustrates critical flux and limiting flux, which reveals the filtration performance of a given dispersion. In this study, the filtration characteristics of Laponite dispersions with and without applying ultrasound at three cross-flow fluxes were compared. Results are given using the parameter J_v/Lp (the ratio between the permeate flux and the permeability of membrane, Pa) in order to minimize the deviation of the permeate flux arising from variations in membrane permeability (variable from 74.2×10^{-5} $L.h^{-1}.m^{-2}.Pa^{-1}$ to 94.6×10^{-5} $L.h^{-1}.m^{-2}.Pa^{-1}$).

During the filtration of Laponite dispersions (0.48 vol%), the evolution of permeate flux Jv, inlet (P_{in}) and outlet (P_{out}) pressures of filtration cell and cross-flow flux Qv over time were monitored, and are displayed in Fig. 3. Filtrations at three Qv (0.2 $L.min^{-1}$, 0.45 $L.min^{-1}$ and 0.6 $L.min^{-1}$) were performed both with and without ultrasound. Taking an average dispersion viscosity at high shear rates, $\mu = 0.003$ Pa.s, Reynolds numbers without ultrasound can be calculated at 184, 414 and 552 for Qv = 0.2, 0.45 and 0.6 $L.min^{-1}$ respectively, which shows that these dispersions are in the laminar flow regime. The steady-state curves of Jv/Lp versus applied transmembrane pressure TMP (average of P_{in} and P_{out}) were then drawn according to the permeate flux at steady states of every filtration step (Fig. 4). At the beginning, a low transmembrane pressure TMP = 0.2×10^5 Pa is applied which yields a certain permeate flux J_{v1}. TMP is then increased to 0.5×10^5 Pa, once the steady state is reached, it is decreased again to 0.2×10^5 Pa so that the new permeate flux J'_{v1} could be compared with J_{v1} for the purpose of differentiating possible deposit formation from a reversible concentration polarization layer. These coupled permeate fluxes at every TMP are denoted J_{v2}-J'_{v2}…J_{v5}-J'_{v5}. As shown in Fig. 3a and 4, J'_{vn} is mostly equal to J_{vn} during the three filtrations without ultrasound, which indicates that reversible concentration polarization is the dominant phenomenon rather than irreversible deposit formation in this state of filtration. Interestingly, the permeate flux increases steadily from a very low level every time the pressure is lowered, and it decreases from a very high level once the pressure goes up (Fig. 3a). According to Pignon et *al.* [21], this could be explained by a reversible deposit that is formed as the rise of TMP and which is then eroded by shear-induced hydrodynamic forces when the pressure is released. In addition, a so-called limiting flux is reached very quickly at the very beginning of filtration, since the permeate flux hardly raises whatever TMP increases until 1.4×10^5 Pa. The limiting fluxes are 19 $L.h^{-1}.m^{-2}$ at Qv = 0.6 $L.min^{-2}$ (Fig. 3a) and 14 $L.h^{-1}.m^{-2}$, 8 $L.h^{-1}.m^{-2}$ at Qv = 0.45, and 0.2 $L.min^{-2}$, respectively (results not shown). The appearance of limiting flux implies that the concentrated particles layer is dense even though it is reversible.

Figure 3b demonstrates that the application of ultrasound leads to an immediate increase of permeates flux, and that steady states can be reached almost immediately after every operation below 1.1×10^5 Pa. As discussed before, the arc-like shapes in Fig. 3a are related to formation/erosion of a reversible deposit, which implies that no such deposit could be formed under ultrasonication since the evolution of permeate flux follows a constant-deviation regime at these TMP (from 0.2×10^5 Pa to 1.1×10^5 Pa). When TMP further increases to 1.4×10^5 Pa, a slight-depleting curve of permeate flux is observed, indicating a formation of a accumulated particles layer, but a much more thinner one than without ultrasound. In addition, those coupled permeate fluxes J_{vn}-J'_{vn} are equal to each other owing to the non-existence of irreversible deposit.

In order to better assess the effect of ultrasonication on filtration performance of Laponite dispersions, two additional cross-flow fluxes (0.2 $L.min^{-1}$, 0.45 $L.min^{-1}$) were applied. Though the filtration curves of these two experiments are not presented here, steady-state curves have all been assembled in Fig. 4. In general, the application of ultrasound leads to a significant increase of permeate flux, from 3 to 5 times, during filtrations of Laponite 0.48 vol% at three Qv. Moreover, different filtration behaviors have been observed: instead of being limited, the permeate flux continues to increase with TMP up to 1.4×10^5 Pa for all three filtrations under ultrasonication. Since this limiting flux strongly depends on a dense accumulated particles layer, we infer that the applied ultrasonic waves allow reducing this dense concentrated layer.

It also seems that there is a competition/combination between the effect of ultrasonication and that of cross-flow flux Qv, since the observed permeate flux are mostly the same at 0.45 $L.min^{-1}$ and 0.6 $L.min^{-1}$ under ultrasonication. In fact, during conventional filtration, an increase of permeate flux is currently observed with the increase of Qv. It should be noted that the formation of concentrated particles layer during cross-flow filtration results from a balance between the transmembrane pressure TMP and the shear-induced hydrodynamic force in the filtration channel, which is determined by the cross-flow flux. The applied ultrasonic waves in this study provoke only mechanical effects because of their low frequency. We assume, therefore, that the ultrasonication enhances the hydrodynamic force and a maximum in the filtration channel has been reached at certain Qv (between 0.2 $L.min^{-1}$ and 0.45 $L.min^{-1}$) so that a successive increase of Qv does not affect it any more.

This assumption can also explain the evolution of permeate flux curves in Fig. 3b. In this figure we notice that the permeate flux evolution with time reaches an almost constant value for TMP < 1.4×10^5 Pa (for example at time t = 180 min), while the permeate flux slightly decreases over time for TMP = 1.4×10^5 Pa (at time t = 310 min).

We can interpret these evolutions as follows: at TMP < 1.4×10^5 Pa, no additional accumulation of particles occurred in these steps. (Nevertheless the permeation flux was lower than the one for clean water, indicating a possible irreversible fouling layer at the membrane surface.) The filtration channel

had a certain level of hydrodynamic force with a constant Qv and stable ultrasonication, the increase of TMP would result in a reinforcement of convection flux towards the membrane leading to an instantaneous concentrated particles layer, which could be then fluidized by shear-induced hydrodynamic diffusion. Once the convection flux towards the membrane was so important that the instantaneously formed concentrated layer could not be totally fluidized by the hydrodynamic force, a steady concentrated particles layer would appear while the permeate flux decreased over time, as the case here at TMP = 1.4×10^5 Pa (at time t = 310 min).

In this section, macroscopical effect of ultrasonication on cross-flow filtration has been revealed. A high efficiency of ultrasonication to increase the filtration performance of Laponite dispersions has been shown, in the case that it is applied directly to the dispersions on the feed side of the membrane. In addition, no membrane damage was observed since membrane permeability remains stable after every ultrasonic-assisted filtration. No heating effect was observed due to the application of ultrasound neither, since the average temperatures at both inlet and outlet of filtration cell were around 25 °C, as presented in Table.1. By measuring dry weight percentage of feed and permeate, the rejection rate of membrane has also been determined and the results are listed in Table 1. According to these results, application of ultrasound did not change the rejection rate of the used PES membrane.

3.3 Colloidal organization at nano-scale during ultrasonic-assisted cross-flow filtration

In order to confirm the hypothesis that applied ultrasonic waves have reduced concentrated particles layer during filtration, *In-situ* SAXS measurements were carried out during cross-flow filtration, with two volume fractions of Laponite dispersions (Φv = 0.48 vol% and Φv = 1 vol%). To ensure some marked accumulated particles layer so as to emphasize the effect of ultrasonication, only the more concentrated one (1 vol%) will be presented in the following.

3.3.1 Concentration calibration and SAXS analysis

Static SAXS measurements were performed in the capillary flow-through cell at 25±1 °C to establish a calibration curve. The results of the scattered intensity as a function of volume fractions allows us to define the following linear relationship (Fig. 5): I (q = 1.2 nm^{-1}) = 0.0497 Φv. This equation has been established in the linear zone of the scattered intensity (q^{-2} power law decay) corresponding to the form factor of the dispersions, which indicates that it is not affected by the increasing mutual particle interaction (describing by the structure factor of the dispersions) and therefore valid at high dispersion concentrations [21].

With the obtained calibration curve, the volume fraction of any Laponite dispersion could be determined by introducing the corresponding absolute scattered intensity at a scattering vector q = 1.2 nm^{-1}. This method has already been used [21,29,32,33] to determine the evolution of the concentration of the dispersions as a function of the distance z from the membrane. In other words, the concentration profiles in the accumulated layers during filtration are determined by this method. The scattering intensity for all the volume fractions reached within the concentrated particles layers at scattering vector q = 1.2 nm^{-1} are in the q range where the scattering intensity is not affected by neither the structure factor nor the possible anisotropy of the SAXS pattern, as already discussed in precedent work [21].

3.3.2 Effect of ultrasonication on concentrated particles layer at steady state

After the introduction of Laponite dispersions at initial ϕv = 1 % in the ultrafiltration vessel, several hydrodynamic parameters were explored and the ultrasound was applied during certain steps of filtration. At TMP = 1.1 $\times 10^5$ Pa, two successive cross-flow fluxes were explored as presented in Figure 6. When Qv = 0.2 $L.min^{-1}$, the permeate flux at steady state is always around 5.5 $L.h^{-1}.m^{-2}$; it then increases to around 8.5 $L.h^{-1}.m^{-2}$ at Qv = 0.3 $L.min^{-1}$, no difference of permeate flux is observed among the filtration steps without ultrasonication (steps 1, 3 and steps 5, 7, 9).

Once the ultrasonic waves are applied, the permeate flux is reinforced immediately (Fig.6). The first ultrasonic application (step 2) leads to an increasing of permeate flux from 5.5 $L.h^{-1}.m^{-2}$ to 29 $L.h^{-1}.m^{-2}$ progressively. The second one (step 4) then brings the flux up to 45 $L.h^{-1}.m^{-2}$ also progressively but the equilibrium state is reached more quickly. As for the next filtration steps with ultrasound, the permeate flux increases instantaneously when the ultrasound is applied, and they are then brought to 75 $L.h^{-1}.m^{-2}$ and 90 $L.h^{-1}.m^{-2}$ (average) for step 6 and 8 respectively at Qv = 0.3 $L.min^{-1}$.

In order to clarify the relative effects of ultrasonication and increase of cross-flow flux, another filtration run following the same procedure from step 1 to step 4 was carried out with Qv = 0.3 $L.min^{-1}$ using a fresh sample (results not shown). The permeate flux curves evolve very similarly between those two runs and the obtained increase in permeate flux are very comparable for different Qv. This clearly shows that, in such a situation, the effect of ultrasounds dominates over that related to changes in Qv.

Figure 7 presents the corresponding concentration profiles at steady state for every concerned filtration steps (measured simultaneously with permeate flux). In accordance to the increase of permeate flux, no more concentrated layer has been found at the end of the steps with ultrasound (Step 2, 4, 6, 8): the volume fractions equal 1 %, i.e. the volume fraction of feed Laponite dispersions, from z = 20 µm to the bulk dispersions. Interestingly, at the end of the steps without ultrasonication (Step 1, 3, 5, 7, 9),

lower concentrations for all the distances z are exhibited at the following step than the precedent ones: the concentrated particles layer is thinner and less concentrated at step 3 compared to step 1 although the experimental parameters (Qv = 0.2 $L.min^{-1}$, TMP = 1.2×10^5 Pa) are the same; similar observations can be made for steps 5 and 7. Furthermore, this decrease in concentration seems to be slowing over time since almost equal concentration profiles have been observed for step 7 and 9.

It should be noted that the Laponite dispersion has an attractive network that consists of sub-units of particles, micron-sized aggregates formed from a dense stack of sub-units and a fractal mass consisting of a loose mass of micron-sized aggregates [23–25]. During filtration, a denser aggregates and more connected gel forms the concentrated particles layer which limits the permeate flux [25]. On the basis of the knowledge of this global structural organization, we can speculate the effect of ultrasonication on the structural modification of these dispersions. It seems that the applied ultrasonication is able to disaggregate this dense network like an additional force but it takes time to complete such a disaggregation. This could explain why different scenarios for increasing permeate flux are observed: at step 2, the ultrasonic waves began to break up the dense aggregates and the connection among them (mass fractal) formed since step 1. There should be however, always some dense and highly connected aggregates in the accumulated particles layer so that the mechanical effect of ultrasound was restricted, hence, the permeate flux increased slowly. During step 3 when ultrasonication was stopped, the fragments of aggregates, the aggregates not yet disassembled could re-accumulate on the membrane surface; they could be further disaggregated by ultrasonic waves at step 4. Since the accumulated particles layer became looser due to the partial disassembling of aggregates, the ultrasonic waves could find a pathway more easily to disrupt the concentrated layer more quickly. Consequently, the permeate flux of this step increased much faster than step 2. Presumably, all the dense aggregates have been completely disassembled at the end of this step since the permeate flux increased instantaneously at the next ultrasonication step, suggesting that there was no more restriction of the remaining dense aggregates to prevent ultrasonic action within the concentration layer.

In addition, the fact of partial disassembling of aggregates could probably explain the different permeate flux values at steady state among the ultrasonication steps. At the end of step 2, 4 or 6, no concentrated particles layer remained at the concerned position of the channel but the dispersion could still consist of some loose mass of micron-sized aggregates, which were not visible in this concentration analysis (scattered vector q = 1.2 nm^{-1} , corresponding to a length of 5 nm), restricting the mass transfer of filtration. These loose aggregates could be further disassembled at every ultrasonication step until a uniform state: sub-units of clay particles. Hence, the values of permeate flux are higher at the following ultrasonication step than the precedent ones.

3.3.3 Temporal effect of ultrasonication on concentrated particles layer

3.3.3.1 Break-up of concentrated particles layer under ultrasonication

The application of ultrasound appears to lead to a disruption of concentrated particles layer resulting in an increase of permeate flux. It is then particularly important to try to know how this concentrated layer has been disrupted. With this purpose, the evolution of concentration profiles over time has been investigated for every filtration step. Evolutions of concentration profiles at steps 2, 4 and 6 (with ultrasonication) are presented in Fig.8. As shown in Fig.8a, at Qv = 0.2 $L.min^{-1}$, it takes 100 min for the first ultrasonication (step 2) to completely remove the accumulated particles layer. As described in the former section, the dense structural organization of particles should be disrupted by ultrasonic waves at step 2 so that the second ultrasonication (step 4) takes only 20 min to remove this reformed concentrated layer. For the same Qv, the layer at step 4 is looser and less concentrated (but with the same thickness) than the one of step 2, shown in Fig.8b. When the cross-flow flux increases to 0.3 $L.min^{-1}$, it takes 13 min to remove the whole concentrated particles layer, resulting from both continuous disaggregation by ultrasound and reinforcement of shear-induced hydrodynamic force by the increase of Qv (Fig.8c).

One explanation for these different break-up times could be, that during the first ultrasonication step (step 2), the ultrasonic action was restricted within the concentrated particles layer arising from the viscous, highly-aggregated dispersions. For instance, the formation and implosion of cavitation bubbles were difficult (high threshold of cavitation owing to high viscous medium) and it was also difficult to find a pathway to create acoustic streaming. At the following ultrasonication steps (step 4 and 6), the dispersions were more disaggregated so that the threshold of cavitation drops off and acoustic streaming was strengthened thanks to the decrease of viscosity. As a consequence, the break-up time significantly decreases.

Kinetic data on concentrated particles layer break-up by ultrasonication are presented in Fig. 9. Different distances in this layer, 20 µm, 60 µm, 100 µm, 220 µm and 320 µm from the membrane surface were selected. For the three concentration profiles (Fig.8) and for each distance, the evolutions of volume fractions with time were determined. At the first ultrasonication step (step2, Fig.9a), the volume fractions decrease at a similar rate below 100 µm, and they drop off more rapidly than those at higher distance. This indicates that the bottom of the concentrated particles layer (close to the membrane) is the target zone of disruption under ultrasonication. The same conclusion can be drawn for the second ultrasonication step (step 4, Fig.9b).

It also appears that the break-up regime is not regular with time at step 2: volume fractions drop with variable velocities, they even start to increase at 77 min for all distances z within the concentrated particles layer, probably owing to the re-balance between the detached gel from others parts of the channel and the remaining concentrated layer of concerned section. Since the measurements were carried out in the middle of the filtration cell (x = 50 mm), it is possible that at 77 min, detached gel

from other parts was brought by ultrasound-induced turbulence and added rapidly into the remaining layer driven by pressure gradient.

Otherwise, the concentration profiles at step 2 and 4 (Fig. 8a and 8b) are of regular form without sign of disruption. In fact, they follow an exponential shape like those without ultrasound, as described in section 3.3.3.2. These observations could be explained by the effective range of ultrasonication: the actions induced by ultrasonication should be on the order of micrometers even smaller so that the disruption of concentration profile is invisible for measurements performed every 20 µm. However, when the cross-flow flux increases to 0.3 $L.min^{-1}$, the concentration profiles are not regular any more, it seems that the concentrated layer has been subjected to a force of agitation. (Fig. 8c). For example at time t = 9 min, the evolution of Φv (z) does not follow a continuous decrease. Evidences can also be found in Fig.9c: the volume fraction drop is irregular and very rapid. Firstly, we should note that at step 6 the dispersions have already been subjected to the ultrasonication for quite a while so the disaggregation should be more complete, which made the ultrasound more effective in this medium, for example with more pronounced action of acoustic streaming. Furthermore, the hydrodynamic force was enhanced by increasing the cross-flow flux. Therefore, it should be the combined action of these two factors as the origin of the rapid break-up with the irregular distribution of the concentration as a function of z.

3.3.3.2 Growth of concentrated particles layer after ultrasonication

Figure 10 presents the growth of polarization layers after ultrasonication at Qv = 0.2 $L.min^{-1}$ and 0.3 $L.min^{-1}$ (Step 3 and 5, respectively). At the transient state, colloidal matter accumulates to the membrane progressively. Even though the two concentration layers at steady state are different, a complete growth takes 45 min for both of them. This indicates that the effect of ultrasonication on filtration is almost instantaneous: the accumulation of matter at membrane surface can not be attenuated when ultrasonication is switched off. In addition, the accumulated layers follow an exponential shape over distance z at any given time during filtration: $\mathbf{\Phi v}\ (z) = \alpha.\exp(-\beta \mathbf{z})$, where α is the volume fraction at z = 0 µm, and β defines the curve steepness. The higher the value of β is, the steeper the curve. Similar behavior is also observed for colloidal dispersions in drying process [34]. It appears that the concentration profiles at Qv = 0.3 $L.min^{-1}$ are steeper and the accumulated layers are thinner than those at 0.2 $L.min^{-1}$ (thickness of the accumulated layer varies from 220 µm at 0.3 $L.min^{-1}$ to 420 µm at 0.2 $L.min^{-1}$). The reinforcement of Qv thins the accumulated layers but it seems that it has a reduced influence on the layers closer to the membrane.

The growth kinetics of concerned accumulated particles layers are presented in Fig. 11. For the position nearest from the membrane surface, growth kinetics can be modeled by the following

exponential relationship: $\mathbf{\Phi v}$ (t) = m_1+m_2.(1-exp(-m_3**t**)), where m_1 is the initial volume fraction at t = 0 min, m_2 defines the amplitude and m_3 describes the growth rate of the volume fraction Φv over time. Curve fittings were performed only for the concentrated particles layers at z = 20 µm, 60 µm and 100 µm, and the parameters illustrate the growth behaviors at different Qv. For both applied Qvs, the accumulated particles layers close to the membrane (ex. z = 20 µm) grow faster than those far from the membrane (ex. z = 100 µm). However, the growth rates m_3 of accumulated layers are distinct at different Qv. At Qv = 0.2 L.min^{-1}, the layers within 100 µm develop with a slightly changed growth rate, m_3 varies from 0.060 to 0.045. At Qv = 0.3 L.min^{-1}, the layer close to the membrane (z = 20 µm) grows 3 times faster than that far from the membrane (z = 100 µm), which grows even faster than the layer of the same position at Qv = 0.2 L.min^{-1} (m_3 value: 0.100 VS 0.060).

As mentioned in the previous section, the balance between transmembrane pressure and shear-induced hydrodynamic force determines the formation of polarization layer during cross-flow filtration. The increase of cross-flow flux from Qv = 0.2 L.min^{-1} to 0.3 L.min^{-1} enhanced the hydrodynamic force so that the growth of concentrated particles layer far from the membrane surface (z = 100 µm) was slowed down (m_3 varies from 0.045 to 0.034). However, it seems not to slow down but speed up the accumulated layer growth near the membrane since the growth rate at 20 µm increases with the applied cross-flow flux. This could be interpreted by the fact that more particles have been brought during the same time interval by the enhanced cross-flow flux. Consequently, in taking account the observations in Fig.10, it seems not to the best efficient way to increase cross-flow flux Qv for removing the polarization layer from the membrane surface.

3.3.4 Spatial effect of ultrasonication on polarization layer

Three windows of measurements are available, located at 7 mm, 50 mm and 93 mm from the filtration cell entrance (see section 2.3.1).

To obtain concentration profiles, we then started with a matrix of 3 columns (x axis, distance from the filtration cell inlet) and 20 rows (z axis, distance from the membrane) with concentration data points. The graphing software ORIGIN 8.5 was then used to sketch this contour by a four step process: creating Thiessen (Delaunay) triangles in the XY plane; linear interpolation; drawing of contour lines and smoothing. Fig. 12 presents the contour charts of filtration channel during cross-flow ultrafiltration of Laponite dispersions (1 vol%) with and without ultrasound considering a continuous and linear evolution between the three measurements points. SAXS measurements were carried out every 20 µm from the membrane (first point of measurement: z = 20 µm). As depicted in Fig. 12a, at steady state of filtration without ultrasonication, the thickness of the concentrated particles layer increases along the filter surface (x axis): no layer is observed at x = 7 mm and a layer of 200 µm is

formed at x = 50 mm, this layer then accumulates to 300 µm at x = 93 mm. In addition, local particle volume fraction increases at every distance z within the accumulated layer along x. For instance, at 20 µm from the membrane surface (z = 20 µm), it is 1 vol%, 2.5 vol% and 2.7 vol% at 7 mm, 50 mm and 93 mm, respectively. These observations by *in-situ* SAXS measurements have allowed for the first time, to highlight the existence of concentration distribution along the membrane in accordance to theoretical cross-flow filtration models. Researchers [35–38] have predicted such an axial dependence of particle layer. According to them, a polarized layer could attain a thickness that is constant in time but increases with distance from the filter entrance, which gives rise to a stable permeate flux at steady state. This steady state is maintained by convective motion of permeate through the membrane and shear-induced hydrodynamic diffusion along the membrane. Romero and Davis [36] also pointed out that a stagnant, concentrated layer beneath the flowing layer could form from certain position and the local permeate velocity decreases along the filter surface.

An ultrasonication of 20 kHz and 2 $W.cm^{-2}$ was then applied. In Fig. 12b, the contour chart after ultrasonication of 1 hour shows a significant disruption of this polarization layer. Concentration profiles are homogeneous for all distances z at x = 7 mm as well as 50 mm, with the feed concentration (1 vol%). At x = 93 mm, the volume fractions of Laponite decrease 30% when close to the membrane and 1.9 vol% is attained at z = 20 µm. It is also worth mentioning that, at this x position, ultrasonication does not significantly reduce the thickness of the polarization layer. Similar trends were already noticeable in Fig.8. It then appears that in the transient state, the volume fractions of the whole accumulated layer decreases while maintaining a constant layer thickness. Erosion of this layer only starts once a sufficiently low critical volume fraction is reached. Therefore, it could reasonably be inferred that this disrupted layer in Fig 12b will be thinned over time. We could also ask if this critical volume fraction corresponds to one threshold state of dispersions (with certain yield stress and structural organization) for which the combined effect of shear flow and ultrasonication is sufficiently high to disrupt the layer by mechanical erosion (thickness reduction).

4. CONCLUSIONS

This work combines macroscopic results with simultaneous nanometric observations of phenomena during ultrafiltration assisted by ultrasound. It is the first time that the ultrasonic effect on cross-flow filtration was investigated by *in-situ* characterizing the concentration profiles and structural organization within concentrated particles layer.

Firstly, this research has shown that a simultaneous ultrasonication of 20 kHz could be an efficient way to improve cross-flow filtration of Laponite dispersions: it has led to a significant increase of

permeate flux, which can be explained by a progressive break-up of concentrated particles layer, as evidenced by *in-situ* SAXS measurements.

Secondly, the mechanism of ultrasonication has also been discussed. It could be considered as an additional force of an effective range on the order of micrometers or smaller, which is capable to disaggregate highly connected dispersions such as Laponite without modifying their initial particle properties. This progressive disaggregation determines the filtration performance to same extent. In addition, it strengthens the hydrodynamic force of cross-flow ultrafiltration leading to a complete removal of concentrated particles layer.

Finally, in accordance with theoretical predictions, the distribution of concentration profiles along the membrane during cross-flow filtration has been revealed for the first time by experimental observations.

ACKNOWLEDGMENTS

We sincerely thank Jacques GORINI (ESRF, Grenoble), Mohamed KARROUCH, Didier BLESES, Frédéric HUGENELL and Hélène GALLIARD (Laboratoire Rhéologie et Procédés) for technical assistance. We gratefully acknowledge the ESRF for the SC 3483 beam time allocation and Project Cible 2012 of the region Rhônes-Alpes for the financial support.

REFERENCES

[1] S. Sablani, M. Goosen, R. Al-Belushi, M. Wilf, Concentration polarization in ultrafiltration and reverse osmosis: a critical review, Desalination. 141 (2001) 269–289.
[2] W. Gao, H. Liang, J. Ma, M. Han, Z. Chen, Z. Han, et al., Membrane fouling control in ultrafiltration technology for drinking water production: A review, Desalination. 272 (2011) 1–8.
[3] T.M. Qaisrani, W.M. Samhaber, Impact of gas bubbling and backflushing on fouling control and membrane cleaning, Desalination. 266 (2011) 154–161.
[4] V.G.J. Rodgers, R.E. Sparks, Effect of transmembrane pressure pulsing on concentration polarization, J. Mem. Sci. 68 (1992) 149–168.
[5] M. Mayer, R. Braun, W. Fuchs, Comparison of various aeration devices for air sparging in crossflow membrane filtration, J. Mem. Sci. 277 (2006) 258–269.
[6] M.O. Lamminen, H.W. Walker, L.K. Weavers, Mechanisms and factors influencing the ultrasonic cleaning of particle-fouled ceramic membranes, J. Mem. Sci. 237 (2004) 213–223.
[7] I. Masselin, X. Chasseray, L. Durand-Bourlier, J.-M. Lainé, P.-Y. Syzaret, D. Lemordant, Effect of sonication on polymeric membranes, J. Mem. Sci. 181 (2001) 213–220.
[8] J. Li, R.. Sanderson, E.. Jacobs, Ultrasonic cleaning of nylon microfiltration membranes fouled by Kraft paper mill effluent, J. Mem. Sci. 205 (2002) 247–257.
[9] S.R. Gonzalez-Avila, F. Prabowo, A. Kumar, C.-D. Ohl, Improved ultrasonic cleaning of membranes with tandem frequency excitation, J. Mem. Sci. 415 (2012) 776–783.

[10] T. Kobayashi, T. Kobayashi, Y. Hosaka, N. Fujii, Ultrasound-enhanced membrane-cleaning processes applied water treatments: influence of sonic frequency on filtration treatments, Ultrasonics. 41 (2003) 185–190.
[11] M.O. Lamminen, H.W. Walker, L.K. Weavers, Effect of Fouling Conditions and Cake Layer Structure on the Ultrasonic Cleaning of Ceramic Membranes, Sep. Sci. Technol. 41 (2006) 3569–3584.
[12] X. Li, J. Yu, A.G.A. Nnanna, Fouling mitigation for hollow-fiber UF membrane by sonication, Desalination. 281 (2011) 23–29.
[13] H. Kyllonen, P. Pirkonen, M. Nystrom, J. Nuortila-Jokinen, A. Gronroos, Experimental aspects of ultrasonically enhanced cross-flow membrane filtration of industrial wastewater, Ultrason. Sonochem. 13 (2006) 295–302.
[14] S. Muthukumaran, S.E. Kentish, M. Ashokkumar, G.W. Stevens, Mechanisms for the ultrasonic enhancement of dairy whey ultrafiltration, J. Mem. Sci. 258 (2005) 106–114.
[15] K.-K. Ng, C.-J. Wu, H.-L. Yang, C. Panchangam, Y.-C. Lin, P.-K.A. Hong, et al., Effect of Ultrasound on Membrane Filtration and Cleaning Operations, Sep. Sci. Technol. 48 (2012) 215–222.
[16] A. Simon, N. Gondrexon, S. Taha, J. Cabon, G. Dorange, Low-frequency ultrasound to improve dead-end ultrafiltration performance, Sep. Sci. Technol. 35 (2000) 2619–2637.
[17] M. Cai, S. Wang, Y. Zheng, H. Liang, Effects of ultrasound on ultrafiltration of Radix astragalus extract and cleaning of fouled membrane, Sep. Purif. Technol. 68 (2009) 351–356.
[18] R.-S. Juang, K.-H. Lin, Flux recovery in the ultrafiltration of suspended solutions with ultrasound, J. Mem Sci. 243 (2004) 115–124.
[19] A. Mirzaie, T. Mohammadi, Effect of ultrasonic waves on flux enhancement in microfiltration of milk, J. Food Eng. 108 (2012) 77–86.
[20] T. Kobayashi, X. Chai, N. Fujii, Ultrasound enhanced cross-flow membrane filtration, Sep. Purif. Technol. 17 (1999) 31–40.
[21] F. Pignon, M. Abyan, C. David, A. Magnin, M. Sztucki, In Situ Characterization by SAXS of Concentration Polarization Layers during Cross-Flow Ultrafiltration of Laponite Dispersions, Langmuir. 28 (2012) 1083–1094.
[22] R. Avery, J.D. Ramsay, Colloidal properties of synthetic hectorite clay dispersions: II. Light and small angle neutron scattering, J. Colloid Interface Sci. 109 (1986) 448–454.
[23] F. Pignon, A. Magnin, J. Piau, B. Cabane, P. Lindner, O. Diat, Yield stress thixotropic clay suspension: Investigation of structure by light, neutron, and x-ray scattering, Phys. Rev. E. 56 (1997) 3281–3289.
[24] C. Martin, F. Pignon, J. Piau, A. Magnin, P. Lindner, B. Cabane, Dissociation of thixotropic clay gels, Phys. Rev. E. 66 (2002) 021401.
[25] F. Pignon, A. Magnin, J.-M. Piau, B. Cabane, P. Aimar, M. Meireles, et al., Structural characterisation of deposits formed during frontal filtration, J. Mem. Sci. 174 (2000) 189–204.
[26] C. Martin, F. Pignon, A. Magnin, M. Meireles, V. Lelièvre, P. Lindner, et al., Osmotic Compression and Expansion of Highly Ordered Clay Dispersions, Langmuir. 22 (2006) 4065–4075.
[27] A. Magnin, J.M. Piau, Cone-and-plate rheometry of yield stress fluids. Study of an aqueous gel, J. Non-Newt. Fluid Mech. 36 (1990) 85–108.
[28] T. Narayanan, O. Diat, P. Bösecke, SAXS and USAXS on the high brilliance beamline at the ESRF, Nucl. Instrum. Methods Phys. Res., Sect A. 467–468, Part 2 (2001) 1005–1009.
[29] C. David, F. Pignon, T. Narayanan, M. Sztucki, G. Gesan-Guiziou, A. Magnin, Spatial and temporal in situ evolution of the concentration profile during casein micelle ultrafiltration probed by small-angle x-ray scattering, Langmuir. 24 (2008) 4523–4529.
[30] F. Pignon, A. Magnin, J.-M. Piau, Thixotropic behavior of clay dispersions: Combinations of scattering and rheometric techniques, J. Rheol. 42 (1998) 1349–1373.
[31] B. Espinasse, P. Bacchin, P. Aimar, On an experimental method to measure critical flux in ultrafiltration, Desalination. 146 (2002) 91–96.
[32] F. Pignon, A. Alemdar, A. Magnin, T. Narayanan, Small-Angle X-ray Scattering Studies of Fe-Montmorillonite Deposits during Ultrafiltration in a Magnetic Field, Langmuir. 19 (2003) 8638–8645.

[33] F. Pignon, G. Belina, T. Narayanan, X. Paubel, A. Magnin, G. Gésan-Guiziou, Structure and rheological behavior of casein micelle suspensions during ultrafiltration process, J. Chem. Phys. 121 (2004) 8138–8146.
[34] F. Boulogne, L. Pauchard, F. Giorgiutti-Dauphiné, R. Botet, R. Schweins, M. Sztucki, et al., Structural anisotropy of directionally dried colloids, arXiv:1309.1048 [cond-Mat.soft]. (2013).
[35] R.H. Davis, D.T. Leighton, Shear-induced transport of a particle layer along a porous wall, Chem. Eng. Sci. 42 (1987) 275–281.
[36] C. Romero, R. Davis, Global-Model of Cross-Flow Microfiltration Based on Hydrodynamic Particle Diffusion, J. Mem. Sci. 39 (1988) 157–185.
[37] S. Bhattacharjee, A.S. Kim, M. Elimelech, Concentration Polarization of Interacting Solute Particles in Cross-Flow Membrane Filtration, J. of Colloid and Interface Sci. 212 (1999) 81–99.
[38] M. Elimelech, S. Bhattacharjee, A novel approach for modeling concentration polarization in crossflow membrane filtration based on the equivalence of osmotic pressure model and filtration theory, J. of Mem. Sci. 145 (1998) 223–241.

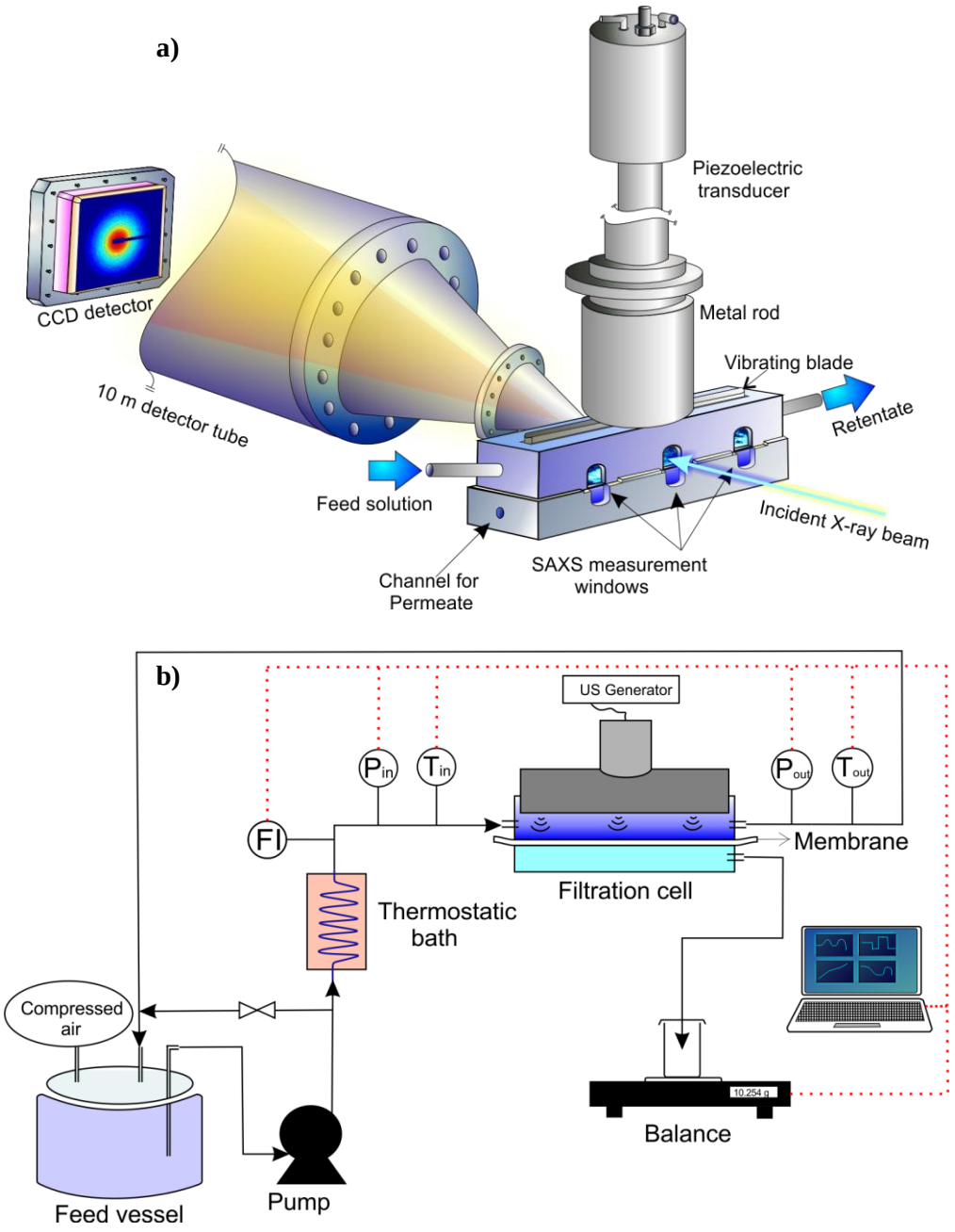

Figure.1. (a) 'SAXS Cross-Flow US-coupled Filtration' Cell during in-situ SAXS measurement; (b) Overview experimental setup of cross-flow filtration

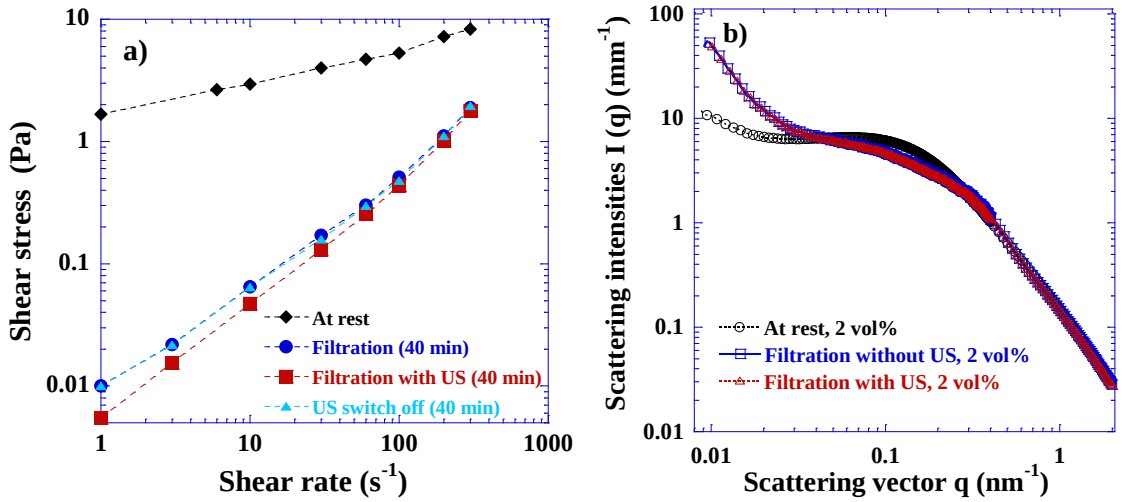

Figure 2. Ultrasonic effect on Laponite dispersions during filtration, tp = 12 days, Cp = 6%, I = 10^{-3} M, pH 10: a) Steady state flow curve at different times of cross-flow filtration (Φv = 1 vol%); b) Comparison of scattering intensities at different conditions. Filtration conditions: T = 25±1 °C, TMP = 1.1×10^{5} Pa, Qv = 0.6 L.min^{-1} (a) and 0.3 L.min^{-1} (b), ultrasound: 20 kHz, 2 W.cm^{-2}.

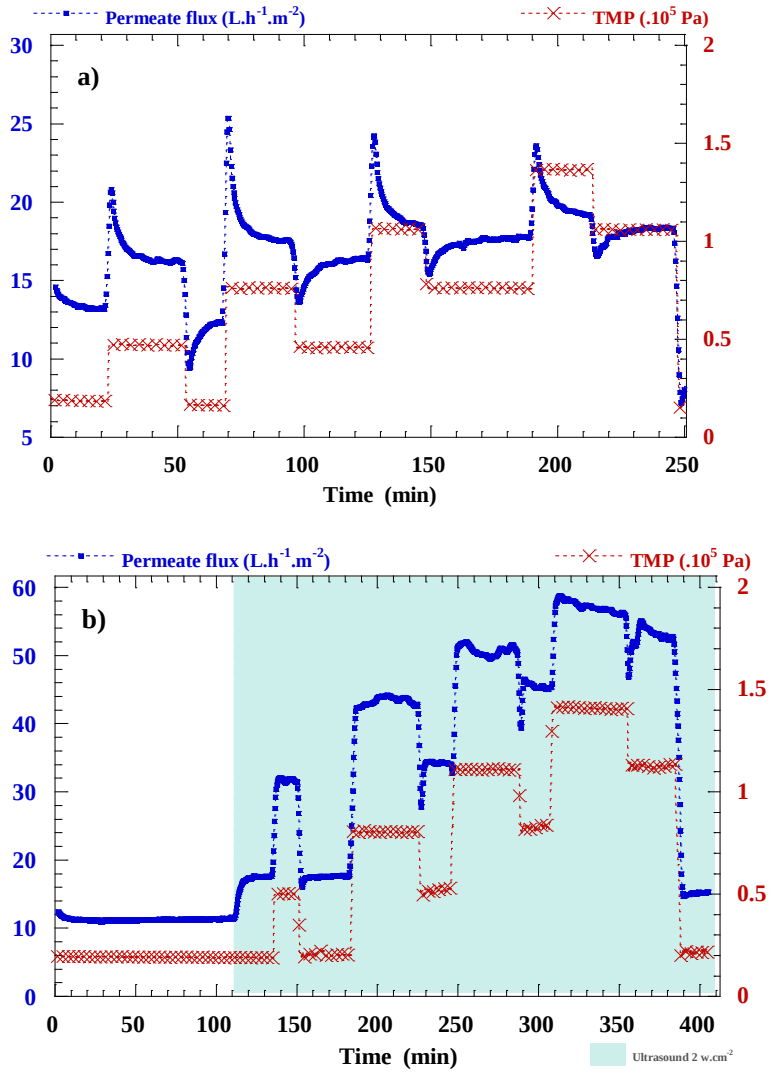

Figure 3.Cross-flow filtration curve by method of Espinasse: evolutions of permeate flux Jv, inlet and outlet pressure of filtration cell $P_{in/out}$ and cross-flow flux Qv over time at Qv = 0.6 L.min^{-1} without (a) and with (b) ultrasonication, the permeability of membrane is 83.1 L.h^{-1}.m^{-2}.bar^{-1}, 94.6 L.h^{-1}.m^{-2}.bar^{-1}, respectively. Laponite dispersions (Φv = 0.48 vol%, tp = 26 days, Cp = 6%, I = 10^{-3} M, pH 10). T = 25±1 °C, Ultrasound: 20 kHz, 2 W.cm^{-2}. Increase of permeate flux obvious; formation of reversible deposit could be avoided under US.

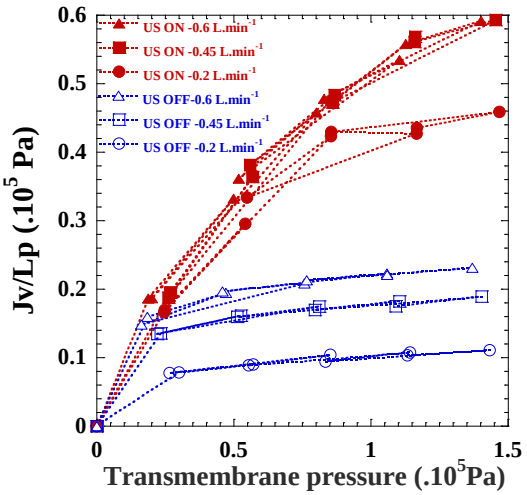

Figure 4. Steady-state curves of J_v/Lp as a function of transmembrane pressure TMP for different Qv with/without ultrasonication during ultrafiltration of Laponite dispersions (Φv = 0.48 vol%, tp = 26 days, Cp = 6%, I = 10^{-3} M, pH 10). T = 25±1 °C, Ultrasound: 20 kHz, 2 W.cm^{-2}. No more limiting flux under US; competitive/combined effect of US and Qv.

Table.1. Average temperatures at inlet and outlet of filtration cell and rejection rates during 250 min's ultrafiltration of Laponite dispersions (Φv = 0.48 vol%, tp = 26 days, Cp = 6%, I = 10^{-3} M, pH 10). Ultrasound: 20 kHz, 2 W.cm^{-2}

Filtrations	**Average temperatures**		**Rejection rate (±3%)**
	Inlet	Outlet	
US ON 0.6 L.min^{-1}	24.97	25.10	94.2%
US ON 0.45 L.min^{-1}	24.92	24.94	95.1%
US ON 0.2 L.min^{-1}	24.88	25.09	93.6%
US OFF 0.6 L.min^{-1}	24.91	24.93	96.6%
US OFF 0.45 L.min^{-1}	25.04	25.31	96.3%
US OFF 0.2 L.min^{-1}	25.11	25.11	97.8%

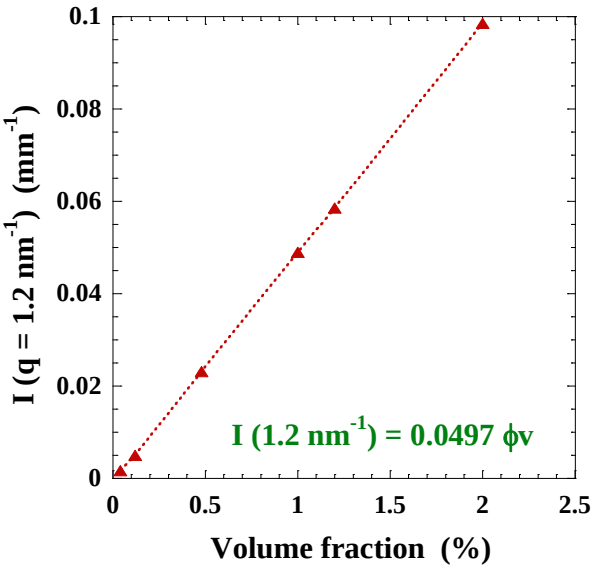

Figure 5. SAXS calibration curve: azimuthal averaged absolute scattered intensity I(q) as a function of volume fraction at particular q vector of 1.2 nm^{-1}. Samples of Laponite dispersions: tp = 12 days, Cp = 6%, I = 10^{-3} M, pH 10, T = 25±1°C.

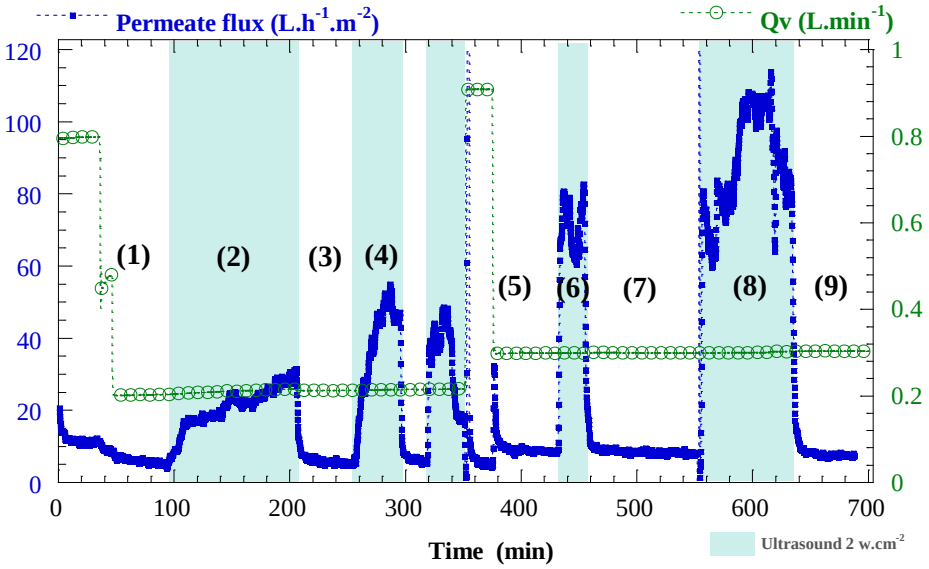

Figure 6. Cross-flow filtration curve: evolution of permeate flux Jv and cross-flow flux Qv over time when the transmembrane pressure TMP = 1.1×10^{5} Pa. Laponite dispersions: Φv = 1 vol%, tp = 12 days, Cp = 6%, I = 10^{-3} M, pH 10. T = 25±1°C. Ultrasound: 20 kHz, 2 W.cm^{-2}. Increase of permeate flux significant; scenarios of permeate flux are different for each step under US.

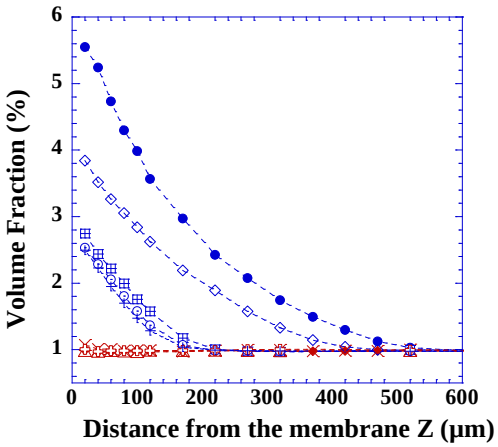

Time (min)	US (W.cm^{-2})	Qv (L.min^{-1})	Step
100	OFF	0.2	(1)
210	2	0.2	(2)
250	OFF	0.2	(3)
300	2	0.2	(4)
430	OFF	0.3	(5)
450	2	0.3	(6)
500	OFF	0.3	(7)
620	2	0.3	(8)
690	OFF	0.3	(9)

Figure 7. Concentration profiles at steady state within the polarization layer deduced from in-situ SAXS during ultrafiltration of Laponite dispersions (Φv = 1 vol%, tp = 12 days, Cp = 6%, I = 10^{-3} M, pH 10) under ultrasonication. T = 25±1°C, TMP = 1.1×10^{5} Pa. Ultrasound: 20 kHz. Concentrated particles layer removal under US; Concentration profiles evolve over time under the same conditions.

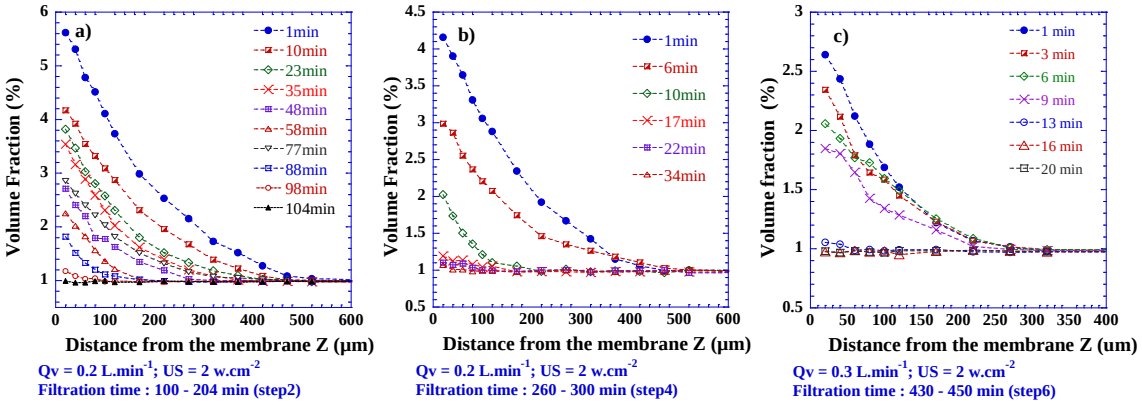

Figure 8. Evolution of concentration profiles within the polarization layer over time during ultrafiltration of Laponite dispersions (Φv = 1 vol%, tp = 12 days, Cp = 6%, I = 10^{-3} M, pH 10) under ultrasonication. T = 25±1°C, TMP = 1.1×10^{5} Pa. Ultrasound: 20 kHz. Break-up time differs from one step to another.

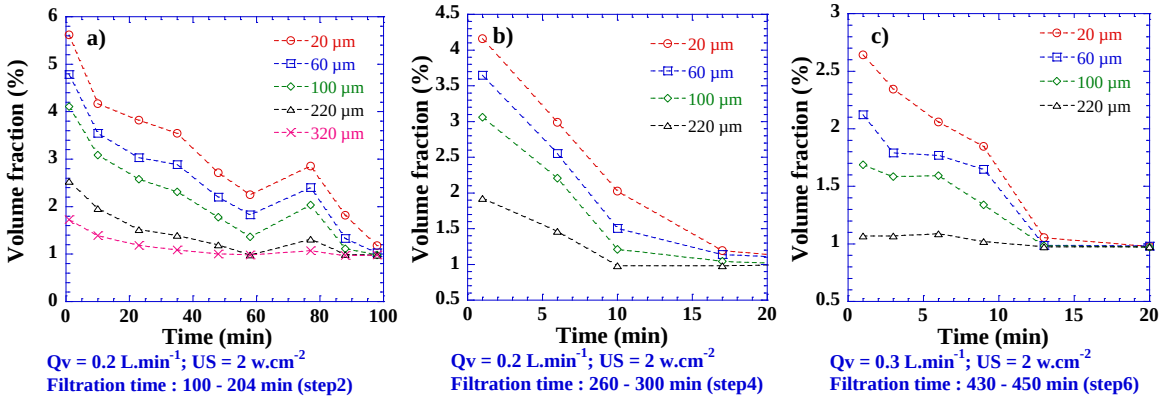

Figure 9. Time evolution of volume fractions at given distance z within the polarization layer during ultrafiltration of Laponite dispersions (Φv = 1 vol%, tp = 12 days, Cp = 6%, I = 10^{-3} M, pH 10) under ultrasonication. T = 25±1°C, TMP = 1.1×10^{5} Pa. Ultrasound: 20 kHz. Bottom of the concentrated layer is the target zone of disruption under US.

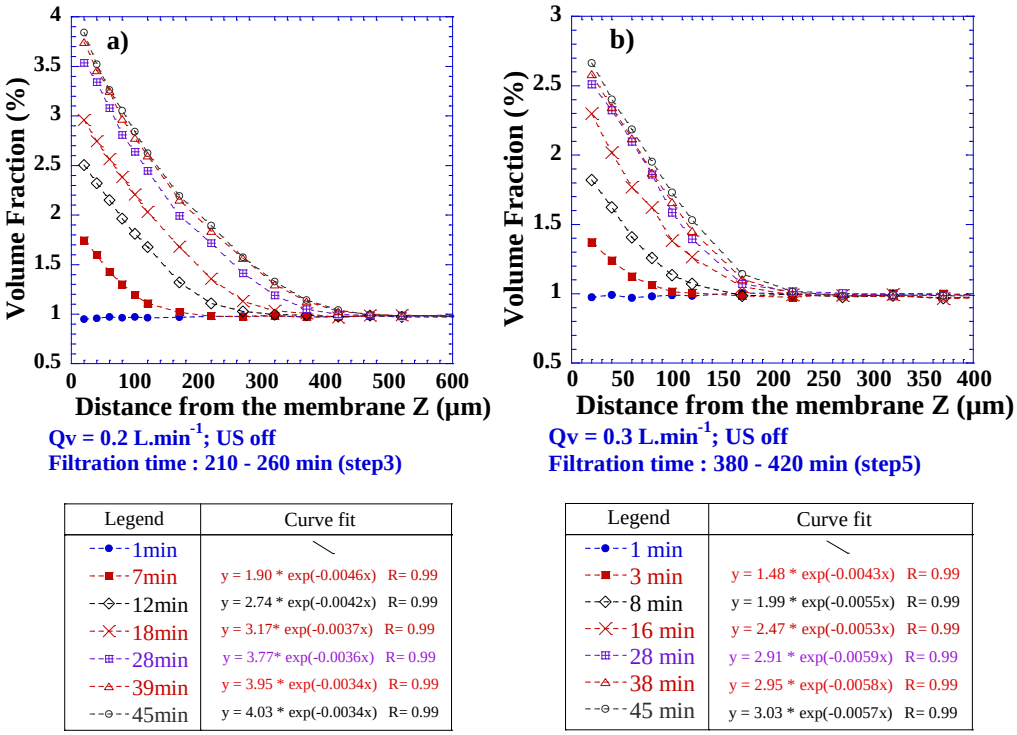

Legend	Curve fit
1min	
7min	y = 1.90 * exp(-0.0046x) R= 0.99
12min	y = 2.74 * exp(-0.0042x) R= 0.99
18min	y = 3.17* exp(-0.0037x) R= 0.99
28min	y = 3.77* exp(-0.0036x) R= 0.99
39min	y = 3.95 * exp(-0.0034x) R= 0.99
45min	y = 4.03 * exp(-0.0034x) R= 0.99

Legend	Curve fit
1 min	
3 min	y = 1.48 * exp(-0.0043x) R= 0.99
8 min	y = 1.99 * exp(-0.0055x) R= 0.99
16 min	y = 2.47 * exp(-0.0053x) R= 0.99
28 min	y = 2.91 * exp(-0.0059x) R= 0.99
38 min	y = 2.95 * exp(-0.0058x) R= 0.99
45 min	y = 3.03 * exp(-0.0057x) R= 0.99

Figure 10. Evolution of concentration profiles within the polarization layer over time during ultrafiltration of Laponite dispersions (Φv = 1 vol%, tp = 12 days, Cp = 6%, I = 10^{-3} M, pH 10) when ultrasound switched off. T = 25±1°C, TMP = 1.1×10^{5} Pa. Concentration profiles follow an exponential shape;

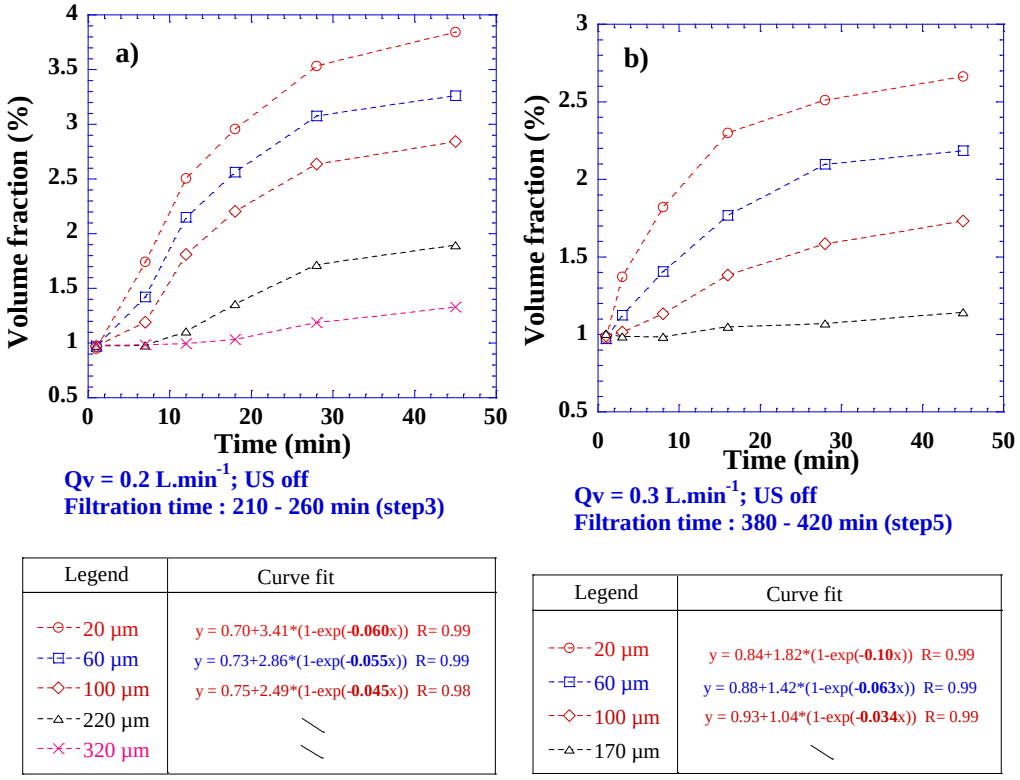

Legend	Curve fit
20 µm	y = 0.70+3.41*(1-exp(-**0.060**x)) R= 0.99
60 µm	y = 0.73+2.86*(1-exp(-**0.055**x)) R= 0.99
100 µm	y = 0.75+2.49*(1-exp(-**0.045**x)) R= 0.98
220 µm	
320 µm	

Legend	Curve fit
20 µm	y = 0.84+1.82*(1-exp(-**0.10**x)) R= 0.99
60 µm	y = 0.88+1.42*(1-exp(-**0.063**x)) R= 0.99
100 µm	y = 0.93+1.04*(1-exp(-**0.034**x)) R= 0.99
170 µm	

Figure 11.Time evolution of volume fractions at given distance z within the polarization layer during ultrafiltration of Laponite dispersions (Φv = 1 vol%, tp = 12 days, Cp = 6%, I = 10^{-3} M, pH 10) when ultrasound switched off. T = 25±1°C, TMP = 1.1×10^{5} Pa.

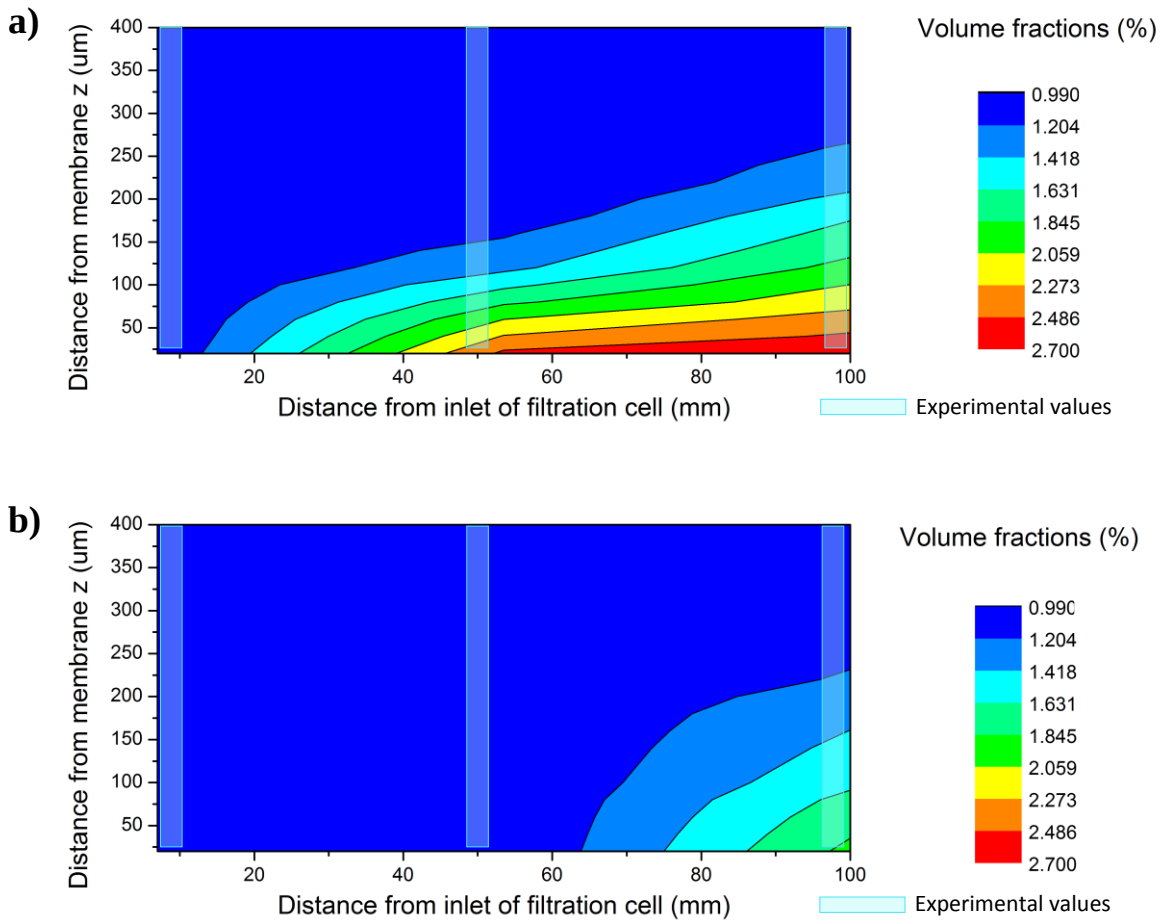

Figure 12. Contour chart of polarization layer in the filtration channel at a given moment during ultrafiltration of Laponite dispersions (Φv = 1 vol%, tp = 12 days, Cp = 6%, I = 10^{-3} M, pH 10) with/without ultrasonication. T = 25±1°C, TMP = 1.1×10^{5} Pa, Qv = 0.3 L.min^{-1}. Ultrasound: 20 kHz, 2 W.cm^{-2}.